Title
Flow heterogeneity following global no-flow ischemia in isolated rabbit heart

Journal
American Journal of Physiology: Heart and Circulatory Physiology, 284(2)

Author
Huesman, Ronald H.

Publication Date
2002-07-01

Flow Heterogeneity Following Global No-Flow Ischemia in Isolated Rabbit Heart

Robert C. Marshall, [1,2] Patricia Powers-Risius, [1] Bryan W. Reutter, [1] Amy M. Schustz, [1] Chaincy Kuo, [1] Michelle K. Huesman, [1] and Ronald H. Huesman [1]

[1]Department of Nuclear Medicine and Functional Imaging, E.O. Lawrence Berkeley National Laboratory, University of California, Berkeley, California 94720-8119; [2]Martinez Veterans Affairs, Northern California Health Care System, Martinez, California 95616

Address Correspondence and reprint requests to:

Dr. Robert Marshall, Department of Nuclear Medicine and Functional Imaging

Lawrence Berkeley National Laboratory

University of California

1 Cyclotron Road, MS55R0121

Berkeley, CA 94720-8119

Phone: 510-486-4265; FAX: 510-486-4768; E-mail: bwreutter@lbl.gov

This work was supported by National Heart, Lung and Blood Institute grants P01 HL25840 and R01 HL60877, and by the Director, Office of Science, Office of Biological and Environmental Research, Medical Sciences Division of the U.S. Department of Energy under Contract No. DE-AC03-76SF00098.

Abbreviated title: Flow Heterogeneity Following Global No-flow Ischemia

Key words: myocardium, microspheres, reperfusion

Abstract

The purpose of this study was to evaluate flow heterogeneity and impaired reflow during reperfusion following 60 min global no-flow ischemia in the isolated rabbit heart. Radiolabeled microspheres were used to measure relative flow in small left ventricular (LV) segments in five ischemia + reperfused hearts and in five non-ischemic controls. Although variable in the post-ischemic hearts, flow heterogeneity was increased relative to pre-ischemia for the whole LV (0.92 ± 0.41 vs. 0.37 ± 0.07, $P < 0.05$)) as well as the subendocardium (Endo) and subepicardium (Epi) considered separately (endo: 1.28 ± 0.74 vs. 0.30 ± 0.09; epi: 0.69 ± 0.22 vs. 0.38 ± 0.08; $P < 0.05$ for both comparisons) during early reperfusion. There were also segments with abnormally reduced reflow. The number of segments with abnormally reduced reflow increased as flow heterogeneity increased.

Abnormally reduced reflow indicates that regional ischemia can persist despite restoration of normal global flow. In addition, the relationship between regional and global flow is altered and venous outflow is derived from regions with continued perfusion and not the whole LV. These observations emphasize the need to quantify regional reflow during reperfusion following sustained no-flow ischemia in the isolated rabbit heart.

Key words: myocardium, microspheres, reperfusion

INTRODUCTION

Compared to *in vivo* hearts, isolated hearts have several advantages for the study of myocardial injury during ischemia and reperfusion. First, flow deprivation is uniform during global no-flow ischemia in *in vitro* hearts since collateral flow is not possible. Second, the presence and amount of physiologic and pharmacological substances in the perfusate that might alter the response of the myocardium to ischemia

and reperfusion can be controlled. Third, because of the systemic effects of a low cardiac output *in vivo*, experimental perturbations that depress cardiac function are more easily studied under sustained, steady-state conditions in isolated hearts. Fourth, the ability to control and measure tracer delivery and prevent recirculation facilitates development and application of tracer methodology to assess flow and metabolism during and following myocardial ischemia. These advantages make the isolated heart an important experimental model to investigate mechanisms that contribute to ischemic and post-ischemic injury as well as interventions to reduce the severity of their damage (29; 32; 37; 45).

One problem in the use of isolated hearts is that quantification of regional blood flow distribution and heterogeneity during reperfusion following global ischemia has received little investigative attention. It has been established that regional blood flow to normoxic myocardium is spatially heterogeneous (3; 5; 7; 8; 14; 19; 27). Similarly, blood flow during regional ischemia and reperfusion is spatially heterogeneous (12; 17; 30). However, blood flow heterogeneity during reperfusion following global, no-flow ischemia is not known. Also, there are conflicting reports about the presence of subendocardial no- or impaired-reflow zones following prolonged complete flow deprivation in isolated hearts (1; 24; 25). If there are zones with impaired reflow following sustained no-flow ischemia, then regionally inadequate post-ischemic blood flow could be a limiting factor determining myocardial salvage in isolated hearts.

The purpose of this investigation was to quantify the effect of 60 minutes of global no-flow ischemia on blood flow distribution and heterogeneity during reperfusion. The experimental preparation was the isolated, isovolumic rabbit heart perfused retrograde with a buffer containing erythrocytes and albumin. Microspheres labeled with different radionuclides were used to quantify regional blood flow before ischemia and during reperfusion. Blood flow heterogeneity was assessed by measuring microsphere deposition in small left ventricular segments. Since accurate measurement of regionally impaired reflow depends on microsphere content, a statistical model was developed to determine the precision with which very low flows could be measured in small myocardial segments containing few microspheres.

Our results indicate that during reperfusion in the isolated rabbit heart: 1) flow heterogeneity is increased relative to pre-ischemia in the left ventricle as a whole and in the subendocardium and subepicardium considered separately; 2) reflow is directed away from the subendocardium into the subepicardium with some myocardial segments receiving impaired reflow; 3) the number of segments with impaired reflow increases as flow heterogeneity increases; and, 4) the extent of reflow heterogeneity and reduced reflow correlate with the intensity of contracture.

The increase in post-ischemic flow heterogeneity and the development of impaired reflow decrease the efficacy with which reperfusion relieves ischemia. In addition, a measured value for global post-ischemic LV flow does not provide information about regional flow heterogeneity, regionally impaired reflow, or the source of venous outflow. These observations emphasize the need to quantify regional coronary reflow in isolated rabbit hearts following sustained no-flow ischemia.

METHODS

Experimental Preparation. All procedures were performed in accordance with institutional guidelines for animal research. Preparation of isovolumic, retrograde erythrocyte and albumin perfused rabbit hearts was similar to previous reports (32; 33). Hearts were obtained from male New Zealand rabbits (R&R Rabbitry, Stanwood, WA) weighing 3.5–4.5 kg. They were given 4000 U heparin sodium (Upjohn, Kalamazoo, MI) and 250 mg pentobarbital sodium (Abbott, North Chicago, IL) via an ear vein. The heart was immediately excised through a median sternotomy, arrested in ice-cold saline, and rapidly attached to a cannula to allow retrograde perfusion. After inserting an apical drain into the left ventricle (LV), a fluid-filled latex balloon connected to a Gould-Statham P23ID pressure transducer (Gould, Oxnard, CA) was inserted across the mitral valve into the LV cavity. The balloon was inflated to maintain diastolic pressure less than or equal to 10 mmHg. Perfusion pressure and systolic and diastolic ventricular pressure were recorded continuously on a Graphtec Linearecorder (Western Graphtec, Irvine, CA). A coronary venous sampling catheter and needle thermistor (Omega Engineering, Inc., Stamford, CT) were inserted into the right ventricle. The venae cavae and pulmonary artery were ligated so all coronary venous drainage flowed out of the sampling catheter. After crushing the atrioventricular node, stimulating electrodes from a Grass SD44 stimulator were placed against the right and left ventricles and 4-V, 4-ms stimuli were delivered at a rate of 180 min^{-1}. Temperature was maintained between 36° and 38°C with a water-jacketed heating coil and heart chamber. Coronary flow was held constant with a peristaltic pump (Rainin Instruments, Woburn, MA). Coronary blood flow rate was measured by timed collection from the venous sampling catheter. Control blood flow rate was approx. 1.4 $ml \cdot min^{-1} \cdot g$ LV wet wt^{-1}. The perfusate was not recirculated.

The perfusate buffer was a modified Tyrode solution that included 5 mM glucose and 2 mM pyruvate, 22 g/L dialyzed, filtered BSA (Fraction V, fatty-acid free, Roche Diagnostics, Indianapolis, IN), and oxygenated bovine erythrocytes (RBCs) adjusted to a hematocrit of 18–20%. The plasma and white blood cell fractions of bovine blood were separated from RBCs by centrifugation. RBCs were oxygenated by multiple spins in perfusate equilibrated with 100% oxygen. The specific electrolyte concentrations of the perfusate buffer were (in mmol/L): 110 NaCl, 2.5 $CaCl_2$, 6 KCl, 1 $MgCl_2$, 0.435 NaH_2PO_4, and 28 $NaHCO_3$. The pH and oxygen tension of the RBC + albumin perfusate were measured using an IRMA™ Blood Gas Analyzer (Diametrics Medical, Inc., St. Paul, MN). The mean ± SDs pH value was 7.39 ± 0.05 and the partial pressure of oxygen was 429 ± 105 mmHg. The flask containing perfusate was gassed with a mixture of 98% O_2 + 2% CO_2 during the experiment.

Regional Myocardial Blood Flow. Regional coronary blood flow was measured with radiolabeled microspheres. Microspheres (mean diameter 15.5 ± 0.1 μm, New England Nuclear Life Science Products Inc., Boston, MA) labeled with cobalt-57, niobium-95, ruthenium-103, tin-113, or gadolinium-153 were suspended in 0.01% Tween-80. The stock solution was prepared by sonicating for about 20 min then vortexing before removing an aliquot for dilution in perfusate buffer. The diluted suspension was vortexed and 0.2 ml was immediately injected over 30 sec into an arterial port 12 cm above the aortic cannula. After the last microsphere injection, the heart was removed from the apparatus and the LV was dissected free, weighed, and plunged briefly into liquid nitrogen. The frozen LV was cut into five rings parallel to the atrioventricular groove. Each ring was cut radially into eight sections (the apical ring into four) using the junction of RV and LV septum for the first section of each ring. Each section was cut into inner (subendocardium) and outer (subepicardium) segments for a total of 72 pieces (92 ± 12 mg, average weight). The location of each piece was recorded and the pieces were weighed in tared vials. The vials were counted on a gamma counter (TM Analytic, Inc., Brandon, FL) enhanced

with a MICRAD automated measurement system (MICRAD, Inc., Knoxville, TN) (33). The computer-based multi-channel-analyzer simultaneously quantified and recorded the spectrum from all isotopes in the sample. Reference standards for each of the five isotopes were also counted. Each sample spectrum was decomposed into a linear combination of the spectra of the reference standards using a weighted least squares fit.

Experimental Protocols

After the heart was prepared, an equilibration period of at least 15 min preceded all experimental interventions. Hearts that generated a systolic developed pressure (peak systolic minus diastolic) greater than 60 mmHg and were stable during equilibration were considered acceptable for use. Developed pressure, diastolic pressure, coronary blood flow rate, and perfusion pressure were recorded after equilibration and prior to each microsphere injection. Intraventricular balloon volume was maintained constant during all experiments. Global no-flow ischemia was produced by clamping the tubing just above the aortic cannula. The temperature of the heart during ischemia was maintained between 36–38°C by wrapping the water-jacketed heart cup and bubbling nitrogen into a saline solution just beneath the heart. At the end of 60 min of ischemia, the tubing was unclamped and flow was re-started and returned to pre-ischemic levels over a 10–12 min interval.

Protocol 1. Reproducibility of Microsphere Technique. The number of microspheres in myocardial segments with very low flows is expected to be considerably less than the "400 microsphere per piece" rule (11). Since reperfusion following 60 min of no-flow ischemia was associated with impaired regional blood flow, the reproducibility of the microsphere technique was tested in two non-ischemic and five post-ischemic hearts by injecting five different radiolabeled sets of microspheres simultaneously (Co-57, Nb-95, Ru-103, Sn-113, and Gd-153). In the two non-ischemic hearts,

microspheres were injected 15 min after equilibration. In the five post-ischemic hearts, microspheres were injected 18 ± 4 min (approx. 20 min) after the start of reperfusion.

Protocol 2. Distribution of Microspheres in Normoxic Myocardium. The spatial heterogeneity and temporal stability of regional myocardial blood flow in normoxic myocardium were assessed by injecting different radiolabeled microspheres at 15 min, 1 hr and 2 hr after equilibration in five control hearts. Coronary flow rates ranged from 0.8 to 1.7 $ml \cdot min^{-1} \cdot g$ LV wet wt^{-1} in individual hearts. The average flow for all five hearts at each injection time is listed in Table 1.

Protocol 3. Distribution of Microspheres in Pre-and Post-ischemic Myocardium. Regional blood flow was measured in five hearts with radiolabeled microspheres just before 60 min of no-flow ischemia and 20 ± 2 min (approx. 20 min or "early" post-ischemia) and 47 ± 4 min (approx. 50 min or "late" post-ischemia) after the start of reperfusion. After initiation of ischemia, the stimulator was turned off when contraction ceased. To reduce the incidence of ventricular fibrillation during reperfusion, the stimulator was not restarted until spontaneous contractions appeared (the two hearts that developed ventricular fibrillation were successfully cardioverted in 2–3 min).

Data Analysis

Calculation of Regional Deposition Density. The deposition density (DD) for each piece of tissue was computed from the concentration of a radiolabeled microsphere in that piece divided by the mean concentration of that microsphere over the entire left ventricle

$$d_i^j = \frac{c_i^j / m^j}{C_i / M} \qquad (1)$$

where d_i^j is the deposition density of isotope *i* in tissue piece *j*, c_i^j is the number of disintegrations of isotope *i* counted from tissue piece *j*, m^j is the mass of tissue piece *j*, $C_i = \sum_{j=1}^{J} c_i^j$ is the total number of disintegrations of isotope *i* counted from the LV, $M = \sum_{j=1}^{J} m^j$ is the total LV mass, and *J* is the number of tissue pieces. Deposition density is the equivalent of relative regional blood flow after mean flow has been normalized to one. The absolute blood flow per unit mass in each sample is equal to the product of deposition density and the mean coronary blood flow to the whole LV. In this study, flow is reported as deposition density instead of absolute flow to allow quantitative comparisons between non-ischemic and post-ischemic hearts perfused at different flow rates.

To display regional deposition density in histogram form, the individual DD values were grouped into bins centered on b_k of width Δb (8)

$$w_{ik} = \frac{\sum_j \left\{ m^j : b_k - \frac{\Delta b}{2} \le d_i^j < b_k + \frac{\Delta b}{2} \right\}}{M} \qquad (2)$$

where w_{ik} is the fractional mass in histogram bin *k* for isotope *i*.

Spatial heterogeneity was expressed as the relative dispersion (RD) and calculated as the weighted sample standard deviation of DD in the tissue pieces, normalized by the weighted mean DD:

$$r_i = \frac{\sqrt{\sum_{j=1}^{72} \left(d_i^j - \bar{d}_i \right)^2 \left(m^j / M \right)}}{\bar{d}_i} \qquad (3)$$

where the weighted mean DD is $\bar{d}_i = \sum_{j=1}^{72} d_i^j \left(m^j / M\right) = 1$ by definition. When computing RD for subendocardium and subepicardium, the weighted mean DD for each layer was used. Comparison of subendocardial (Endo) and subepicardial (Epi) blood flow was computed using the ratio (Endo / Epi) and the difference (Endo–Epi) in control hearts. In the post-ischemic hearts, only the difference was computed because a few subepicardial pieces had very low DD values. Data are expressed as mean ± SDs.

Precision of Flow Measurements. In the Appendix is the statistical model we developed to determine the precision with which very low flows can be measured in small tissue segments containing few radiolabeled microspheres. Sources of statistical fluctuation in microsphere activity measurements include the Poisson probabilistic natures of microsphere entrapment and radioactive disintegration. Using statistical considerations described elsewhere (11; 39), the following estimate of DD measurement variance is derived in the Appendix:

$$Var\left(d_i^j\right) = \frac{M\varepsilon_i\eta_i}{m^j C_i} E\left(d_i^j\right) = \frac{M}{m^j N_i} E\left(d_i^j\right) \qquad (4)$$

where ε_i is the efficiency of counting disintegrations of isotope *i*, η_i is the expected number of disintegrations from a microsphere labeled with isotope *i*, the factor $N_i = C_i / \varepsilon_i \eta_i$ is an estimate of the total number of microspheres labeled with isotope *i* trapped in the LV, and $E\left(d_i^j\right)$ is the expected value of DD corresponding to the relative flow to tissue piece *j*.

According to this scaled Poisson model the DD measurement variance is proportional to the expected value of DD. As a result, absolute precision increases as flow decreases (Fig. 1). For example, if the standard deviation is 0.05 for an expected DD measurement of 1, then the standard deviation will be only 0.025 for an expected DD measurement of 0.25 (i.e., decreasing flow by a factor of four reduces uncertainty by a factor of two). Thus, smaller absolute differences can be discriminated at low flow, compared to high flow. This may be somewhat counterintuitive to the "400 microsphere per piece" rule (11), which is useful for setting the baseline relative precision of non-ischemic flow measurements.

The statistical model developed in the Appendix was tested in the seven Protocol 1 hearts and used to determine the confidence with which microsphere flow measurements indicated impaired reflow.

Criteria for impaired reflow. In post-ischemic hearts, many segments had activities that were much lower than that observed in non-ischemic or pre-ischemic myocardium. Combining measurements from Protocol 2 hearts with the pre-ischemic measurements from Protocol 3 hearts and using only one isotope (Gd-153) from the two non-ischemic hearts in which five differently labeled sets of microspheres were injected simultaneously (Protocol 1), there were 1584 regional blood flow measurements in normoxic myocardium. Seven segments had a deposition density less than 0.1 (0.5%). Based on these observations in non-ischemic myocardium, all segments with deposition densities < 0.1 were considered to have an abnormally low deposition density in post-ischemic myocardium. When analyzing post-ischemic segments for abnormally low deposition density, Equation 4 was used to determine the confidence with which microsphere DD measurements indicated relative flow values < 0.1. As described in the Appendix, this information was then used to calculate the uncertainty in the number of segments having relative flow < 0.1.

Description of Statistics. Data expressed as means ± SDs and regression analyses were performed using KaleidaGraph (Synergy Software) statistical software. Comparisons of functional performance, relative dispersion, and relative blood flow data were performed with Student's two-tailed *t*-test for paired and unpaired observations using StatView statistical software (Abacus Concepts). $P < 0.05$ was considered statistically significant.

RESULTS

Left Ventricular Function and Perfusion. Table 1 lists the mean values for developed pressure, rest pressure, coronary blood flow, perfusion pressure, and coronary vascular resistance for each experimental group. There were no significant differences in any of these parameters when comparing initial values in non-ischemic control hearts to pre-ischemic values in the ischemia-reperfusion groups ($P > 0.2$ for all comparisons). During the 120 min experimental period in control hearts, developed pressure, rest pressure, and coronary flow did not change ($P > 0.2$) while perfusion pressure ($P < 0.03$) increased and coronary vascular resistance ($P > 0.05$) increased insignificantly.

Comparing early reperfusion to pre-ischemia (Protocol 3), developed pressure was severely depressed ($P < 0.001$) while rest pressure ($P < 0.05$) and perfusion pressure ($P < 0.05$) were increased. Coronary blood flow ($P > 0.2$) and coronary vascular resistance ($P > 0.06$) were not significantly different during early reperfusion.

Comparing early and late reperfusion, developed pressure recovered from 32% of pre-ischemic values during early reperfusion to 51% in late reperfusion ($P < 0.02$). Rest pressure ($P > 0.6$) and

perfusion pressure ($P > 0.6$) did not change significantly during reperfusion. Coronary flow ($P < 0.03$) decreased and coronary vascular resistance ($P > 0.06$) tended to increase.

Precision of Flow Estimates with Microspheres (Protocol 1). In accordance with the scaled Poisson statistical model summarized by Equation 4, the observed variance of measurements involving simultaneous injection of five differently radiolabeled sets of microspheres decreased with decreasing DD. Based on initial estimates of the total numbers of microspheres trapped in the LV (the N_i in *Eq. 4*), the observed deviations of the measurements exceeded those predicted by the model by an average of about 27%. Possible explanations for the increased statistical fluctuation include errors in average activity per microsphere reported by the manufacturer (the η_i in *Eq. 4*); deviations in activity from sphere to sphere; errors in our measurements of gamma counter efficiency (the ε_i in *Eq. 4*), due in part to errors in reference standard activities reported by the manufacturer; and sphere aggregation. Using the Protocol 1 heart data, the counter efficiency factors were adjusted as described in the Appendix so that the average observed deviations were within 0.01% of those predicted by the model. Data from other protocols were then analyzed using the adjusted counter efficiency factors.

Flow Heterogeneity and Distribution in Non-ischemic Control Hearts (Protocol 2). Table 2 shows the mean RD values for the whole LV, subendocardium, and subepicardium as well as relative subendocardial and subepicardial blood flow at three different times during 120 min of perfusion in control hearts. RD for the whole LV did not change over 120 min of perfusion ($P > 0.3$). Heterogeneity was insignificantly greater in the subepicardium than the subendocardium at all three time points ($P > 0.1$ for each comparison). Comparing 15 and 120 min values, RD declined 9.1% ($P > 0.1$) for the subendocardium and 20.9% for the subepicardium ($P > 0.1$). Subendocardial DD was increased

compared to the subepicardium, possibly reflecting the presence of an incompressible balloon in the left ventricular cavity. This difference increased with time ($P < 0.03$).

Flow Heterogeneity and Distribution in Ischemic-Reperfused Hearts (Protocol 3). Table 3 shows the values for pre- and post-ischemia RD and the difference between subendocardial and subepicardial relative blood flow for the five hearts subjected to 60 min of ischemia followed by approx. 50 min of reperfusion. The pre-ischemic values for RD and difference in subendocardial vs. subepicardial relative blood flow in these hearts were comparable to the initial values in the control hearts (Table 2) ($P > 0.5$ for each comparison). Comparing early reperfusion to pre-ischemia, there was a marked increase in RD for the whole LV ($P < 0.03$) as well as the subendocardium and subepicardium analyzed separately ($P < 0.05$ for both comparisons). Comparing late reperfusion to pre-ischemia, the increased RD for the whole LV and the subendocardium remained significant ($P < 0.05$ for both comparisons) while the subepicardium was no longer significantly different ($P > 0.1$). The high post-ischemic standard deviations are due to variability in RD values between the five hearts.

Relative blood flow was redistributed from the subendocardium into the subepicardium during early reperfusion ($P < 0.05$). During late reperfusion, this difference was not significant ($P > 0.05$). Comparing late vs. early reperfusion, there was a small reduction in the redistribution of blood flow from subendocardium to subepicardium ($P > 0.1$). The negative values for the difference between subendocardium and subepicardium indicate that, in contrast to pre-ischemia, subepicardial DD exceeded subendocardial flow during reperfusion.

Figure 2 displays in histogram format the mean DD values derived from 12 non-ischemic hearts in which microspheres were injected 15 min after equilibration. Bin width is in 0.1 increments of DD and

the myocardial mass in each bin is expressed as per cent mass for the whole LV (Panel A), subendocardium (Panel B), and subepicardium (Panel C). The distribution of DD (i.e., per cent myocardial mass) is a frequency function of relative blood flow that is centered around the mean normalized value of one. Although there is variation between the curves, all three curves are skewed to the right (skewness of 0.73, 1.20, and 0.89 for LV, subendocardium, and subepicardium, respectively). The LV and subepicardium curves have somewhat flattened peaks (kurtosis of -1.11 and -0.58, respectively), while the peak of the subendocardium curve has a nearly Gaussian shape (kurtosis of -0.04).

Figure 3 shows a DD histogram obtained during early (Panels *A*, *C*, and *E*) and late (Panels *B*, *D*, and *F*) reperfusion from one heart following 60 min of no-flow ischemia. The RD for the LV of this heart was 0.79 and 0.74 during early and late reperfusion, respectively. Compared to non-ischemic hearts, DD is not unimodal about the mean value. Instead, DD is bimodal with markedly reduced reflow to a large fraction of the subendocardium while reflow to the remaining myocardium is widely dispersed with higher peak flows than non-ischemic myocardium (Fig. 2). During early reperfusion, 40.0 ± 3.9% of the subendocardium had impaired reflow. During late reperfusion, 25.3 ± 1.9% had impaired reflow. Subepicardial flow was widely dispersed. There was only one subepicardial segment with reduced reflow during early reperfusion.

All five post-ischemic hearts reperfused for approx. 50 min had qualitatively similar changes. However, quantitatively, there was a wide range of RD values and number of segments with reduced reflow. Compared to the heart in Figure 3, two hearts had flow that was more heterogeneous (average LV RD of 1.35 and 0.91 during early and late reperfusion, respectively) and two had flow that was less heterogeneous (average LV RD of 0.57 and 0.48 during early and late reperfusion, respectively). For

the five hearts combined, 37.5 ± 1.3% of subendocardial segments and 6.0 ± 0.9% of subepicardial segments had impaired reflow during early reperfusion and 27.7 ± 0.7% and 0.8 ± 0.3% had impaired reflow during late reperfusion. Both reflow heterogeneity and impaired reflow tended to decrease as the duration of reperfusion increased.

Figure 4*A* shows the correlation of increased flow heterogeneity and the number of segments with impaired reflow during early reperfusion for the five 60-min ischemia hearts in Protocol 3. Figure 4*B* illustrates the data from the same hearts during late reperfusion. During early reperfusion, the correlation between the number of segments with impaired reflow and RD was $R = 0.91$ for the whole left ventricle and for the subendocardium. For the subepicardium, impaired reflow and RD were poorly correlated ($R = 0.16$). During late reperfusion, the correlation coefficients for the whole LV, subendocardium, and subepcardium were $R = 0.98$, 0.98, and 0.09, respectively. The lack of correlation between the number of subepicardial pieces with impaired reflow and RD was due, at least in part, to the fact that there were very few subepicardial segments with impaired reflow. The positive *X*-intercept indicates that hearts without impaired reflow still have regionally heterogeneous blood flow.

The relationships between flow heterogeneity and impaired reflow vs. intensity of ischemic contracture during early reperfusion were examined in Protocol 1 and 3 hearts (Fig. 5 *A*, *B*). In Protocol 1 hearts, only one isotope (Sn-113) was used to compute RD and number of segments with impaired reflow There was a positive correlation between intensity of contracture and both flow heterogeneity and impaired reflow.

DISCUSSION

Microspheres were used to quantify blood flow distribution and heterogeneity during reperfusion following 60 min of global no-flow ischemia in the isolated rabbit heart. The four most salient findings are: 1) although flow deprivation was homogeneous and absolute, regional flow was more heterogeneous during reperfusion than before ischemia; 2) zones with impaired reflow developed primarily in the subendocardium; 3) the number of LV segments with impaired reflow increased as flow heterogeneity increased; and, 4) the severity of flow heterogeneity and reduced reflow varied between hearts and correlated with the intensity of contracture.

These observations are relevant to the use of the isolated rabbit heart as an experimental model to study ischemia and reperfusion. The abnormal post-ischemic flow distribution adversely affects the efficacy with which reperfusion relieves ischemia. The development of zones with impaired reflow indicates that regional ischemia can persist after reperfusion relieves global ischemia. Also, it is possible that some regions with very high relative flows might be ischemic since the high flows could represent arterial-venous shunting. Since persistent regional ischemia presumably results in continued tissue damage, investigations that use the isolated rabbit heart to study sustained global no-flow ischemia and reperfusion need to quantify post-ischemic regional reflow to assess the efficacy with which reperfusion relieves ischemia.

In addition to persistent regional ischemia, the markedly increased post-ischemic flow heterogeneity changes the relationship between global and regional LV reflow. (Since regional flow has been expressed as deposition density in this study, global LV flow per unit mass corresponds to the mean deposition density value of one.) In normal myocardium, the relationship between global and regional flow is unimodal with regional flows clustered about the mean (Fig. 2). In post-ischemic myocardium,

however, regional flows are widely and unevenly dispersed and are not unimodal about the mean (Fig. 3). The lack of a definable relationship between global and regional flow in post-ischemic myocardium poses two problems. The first is that measured global LV flow provides no information about regional flow distribution. As a result, the return of post-ischemic global LV flow to pre-ischemic levels conceals persistent regional ischemia during reperfusion. Second, since global LV venous outflow is primarily derived from regions with maintained or increased flow, arterial-venous concentration differences do not provide accurate information about either global or regional substrate or tracer extraction. In post-ischemic hearts with heterogeneous regional reflow, accurate measurement of either global or regional substrate and tracer distribution can only be achieved by techniques that directly interrogate the myocardium on a region-by-region basis.

Methodological Considerations. The stochastic nature of microsphere entrapment imposes uncertainty on the relationship between measured microsphere content and expected microsphere content based on true regional flow. Some investigators characterized this uncertainty using relative error, which is computed as standard deviation/mean (4; 11). Since relative error increases as the number of microspheres decrease, the major emphasis of these studies was to define a minimum number of microspheres allowing accurate flow quantification. In an early study, Buckberg et al., (11) reported that 384 microspheres were required for 95% confidence that measured flow was within 10% of true flow. Based on this work, the familiar "400 microsphere per piece" rule was established as a prerequisite for accurate flow quantification. Subsequent studies, however, have shown that fewer microspheres are needed. Nose et al., (39) reported that it was possible to quantify absolute flow with 95% confidence in myocardium containing as few as 49 microspheres as long as the reference sample contained 400 or more microspheres. Directionally similar observations were made by Bassingthwaighte et al., (7; 8). Recently, Polissar et al., (42) reported that global parameters of flow

heterogeneity and correlation coefficients between different sets of microspheres could be accurately measured with less than 400 microspheres per sample.

All of these studies evaluated flow quantification with microspheres in normoxic myocardium. In the present study, there were myocardial regions in post-ischemic hearts with impaired reflow and far fewer microspheres than 400. Nonetheless, microsphere measurements were reproducible and had absolute error that decreased with decreasing flow, in accordance with a Poisson model for microsphere entrapment. To estimate measurement uncertainty, an accurate estimate of the total number of microspheres trapped in the heart is needed. The present study suggests that it is beneficial to perform calibration experiments in which different radiolabeled sets of microspheres are injected simultaneously. Calibration factors can then be checked and adjusted, if need be, for use in estimating uncertainty in subsequent experiments in which only one set is injected at a time.

In small arteries, microspheres tend to enter branches with higher rather than lower flows (7; 8). Microsphere biasing into high flow regions is due to their particulate nature and the greater pressure drop in the direction of higher flow when the vessel diameter approximates the size of the microsphere (15). This bias might have contributed to the increased reflow heterogeneity observed in post-ischemic hearts. Also, intense vasoconstriction or external compression of the microvasculature following ischemia might have exaggerated biasing because the size of the surrounding vessels might have decreased relative to microspheres. Other work has suggested that microsphere biasing is responsible for relatively small errors in normoxic myocardium (7; 8). However, the role that biasing played in the heterogeneous reperfusion in post-ischemic hearts is uncertain: accurate evaluation of microsphere biasing requires comparison to a "molecular microsphere" that is completely extracted and retained in

myocytes under both normoxic and post-ischemic conditions (9). A molecular microsphere fulfilling these requirements has not been identified.

Instead of absolute flow, we assessed regional blood flow as deposition density which is the equivalent of relative regional blood flow after normalizing mean flow to one. Reporting regional blood flow as deposition density has the advantage of allowing quantitative comparisons between hearts studied at different LV perfusion rates. In addition, values for relative dispersion and subendocardial/subepicardial ratios are unaffected using deposition density instead of absolute flow. Since post-ischemic global LV flow tended to be approx. 20% lower than pre-ischemia, deposition density overestimated absolute regional flow during reperfusion relative to pre-ischemia. As a result, the fraction of LV mass with reduced reflow and redistribution of flow away from the subendocardium into the subepicardium was slightly underestimated. These errors were small and did not affect the conclusions of this investigation.

Possible Mechanism(s) for Reflow Heterogeneity. In normal hearts, autoregulation controls the rate of oxygen delivery and the regional differences in oxygen consumption are thought to be responsible for heterogeneous regional blood flow (5; 6; 44; 51). However, in post-ischemic hearts, regionally impaired reflow is not consistent with effective vasomotor control of oxygen delivery, indicating that autoregulation is not the only factor controlling regional blood flow. Ischemic or post-ischemic injury could also affect regional flow distribution with severely injured hearts displaying the most reflow heterogeneity and regionally reduced-reflow. Two observations support this contention: 1) flow heterogeneity and reduced reflow were increased in the subendocardium relative to the subepicardium, consistent with the known vulnerability of the subendocardium to ischemia; and 2) increased flow

heterogeneity and reduced reflow correlated with the intensity of ischemic contracture, an index of ischemic injury.

Ischemic or post-ischemic injury could alter flow distribution during reperfusion by directly injuring the microvasculature. Although originally thought to be a late phenomenon that occurred after myocardial necrosis (28), recent evidence suggests that microvascular injury can occur after only 15 min of ischemia when myocardial injury is still reversible (35). In crystalloid-perfused isolated hearts, microvascular injury appears to involve primarily the endothelium with most of the damage developing after the re-introduction of oxygen during reperfusion (34; 35; 48; 49; 52). Post-ischemic microvasculature injury can increase vascular resistance (18; 49), depress vasodilatory reserve (36; 38), increase capillary permeability to ions (46) and macromolecules (47), alter blood flow distribution (40; 41), and produce endothelial structural changes with bleb formation capable of impeding or obstructing blood flow (16; 20). There is no information to suggest which of these abnormalities (or combination of abnormalities) might have altered post-ischemic flow distribution and heterogeneity in the present study.

Ischemic or post-ischemic injury could also change post-ischemic flow distribution by external compression of the microvasculature due to osmotic swelling or contracture of the surrounding myocardium. Expansion of the extravascular space by osmotic swelling follows a severe ischemic insult and requires at least transient reperfusion. Although the ischemic myocyte does accumulate water due to the osmotic load of intracellular metabolic catabolites (26), extravascular volume does not change or might even decrease during permanent no-flow ischemia (13). Expansion of the extravascular space requires an outside source of water that is supplied with reperfusion. If extravascular expansion is

sufficient to increase intramyocardial pressure, compression of capillaries or post-capillary venules (50) could increase regional resistance to reflow and alter post-ischemic flow distribution.

Contracture also develops following severe ischemic injury (2). By analogy with systolic contraction (21; 43), contracture could increase intramyocardial pressure and compress the microvasculature. Similar to osmotic swelling, if compression of the microvascular is sufficient to increase resistance to regional reflow, flow distribution during reperfusion could be altered (1; 22-24). The positive correlation we observed between contracture and reflow heterogeneity suggests that these two processes might be related. However, a cause and effect association was not established and the nature of that relationship is unknown.

To account for heterogeneous reflow, ischemic injury and microvasculature dysfunction have to be heterogeneous. Since flow deprivation was both homogeneous and absolute, heterogeneous injury can only be accounted for by assuming that vulnerability of the LV to ischemia is heterogeneous. However, the presence and potential mechanism for heterogeneous vulnerability has received little investigative attention. Although it is well known that the subendocardium is more vulnerable to ischemic injury than the subepicardium, increased flow heterogeneity was observed in each of these layers considered separately, indicating that differences between the subendocardium and the subepicardium are not sufficient to account for the present results. Ghaleh et al., (17) observed that heterogeneous infarction was related to pre-ischemic, normoxic flow heterogeneity with higher flow regions suffering more damage than lower flow regions. However, another group of investigators observed that metabolic indices of ischemia were not related to pre-ischemic flow heterogeneity (12). Although myocardial strain is known to be heterogeneous (10), contractile activity stopped at least 10 min prior to any detectable increase in diastolic pressure in all but one heart, suggesting that heterogeneous contraction is

not the sole cause of heterogeneous ischemic injury. Other potential contributors, such as myocyte stress or ion flux and homeostasis, are difficult to measure on a regional basis at a spatial resolution adequate to assess flow heterogeneity. Further exploration of potential mechanisms that could account for heterogeneous injury and heterogeneous reflow following sustained global no-flow ischemia in isolated hearts is needed, in part because the presence and distribution of both ischemic injury and post-ischemic reflow will determine myocardial salvage.

Reflow Heterogeneity, Reduced-reflow, and Ischemia. Based on measurements in non-ischemic myocardium, segments were identified as having abnormally reduced relative blood flow when DD was < 0.1. It is possible that some segments with deposition density < 0.1 might not be ischemic or infarcted. Reduced relative blood flow in non-ischemic segments could reflect severe relative regional contractile dysfunction or altered ion homeostasis with reduced energy consumption following sustained ischemia. Therefore, although reduced reflow does not necessarily identify ischemic or infarcted myocardium, abnormally low relative flow following prolonged absolute flow deprivation does indicate the presence of myocardium that is severely dysfunctional as a result of ischemic damage sustained during no-flow ischemia.

Despite the uniform duration of no-flow ischemia, the intensity of ischemic contracture was variable when comparing individual hearts. To determine if pre-ischemic function or perfusion might be related to the variable ischemic contracture, pre-ischemic coronary flow-rate, perfusion pressure, coronary vascular resistance, and rest and developed pressure were correlated with end-ischemic contracture. There was an insignificant trend for pre-ischemic coronary flow to be inversely related to ischemic contracture ($R = -0.61$, $P > 0.07$). The other parameters were not correlated. Although it is possible that hearts perfused at lower flow-rates might have been under-perfused prior to the initiation of no-flow

ischemia, previous work has shown that lower flows than those encountered here were not associated with detectable high energy phosphate depletion or lactate accumulation (31), suggesting that additional unrecognized factor(s) probably contributed to ischemic injury. Although the reason(s) are not apparent, the variability of ischemic contracture did not adversely affect the conclusions of this investigation. Instead, the correlation between contracture, reflow heterogeneity, and regionally reduced reflow suggests that the severity of ischemic injury might have contributed to the abnormal post-ischemic flow distribution.

Humphrey et al., (24) reported that the presence of an inflated balloon in the left ventricular cavity during ischemia followed by deflation prior to reperfusion allowed the return of normal subendocardial blood flow during the first 20 seconds of reperfusion. However, later studies showed that subendocardial no-reflow developed if reperfusion was continued for longer periods of time (e.g., 5 min) (1; 25). The results of the present study are more consistent with these later studies.

In conclusion, reperfusion following sustained global, no-flow ischemia results in increased regional flow heterogeneity relative to pre-ischemia and the development impaired reflow zones. The severity of abnormal reflow distribution is variable between hearts and correlates with the intensity of ischemic contracture. These observations affect the use of the isolated rabbit heart as an experimental model to study ischemia and reperfusion since; 1) restoration of global flow following sustained no-flow ischemia can be associated with persistent regional ischemia, and 2) arterial-venous concentration differences do not provide reliable estimates of substrate or tracer extraction by the myocardium. Although our observations were made in the isolated rabbit heart, it is possible that similar findings could be detected in hearts from other species.

APPENDIX

A statistical model was developed to determine the precision with which very low flows can be measured in small tissue segments containing few radiolabeled microspheres. Sources of statistical fluctuation in microsphere activity measurements include the probabilistic natures of microsphere entrapment and radioactive disintegration. Using statistical considerations described by Buckberg et al., (11), the number of microspheres trapped in a segment can be assumed to follow a Poisson distribution. Fluctuations in the number of disintegrations detected from a single radiolabeled microsphere obey a second Poisson distribution. However, when the expected number of detected disintegrations is large enough, the variance in counts observed from a segment is due primarily to statistical fluctuations in microsphere entrapment (39).

Entrapment Fraction Calculation. The Poisson statistical model for microsphere entrapment was tested in two non-ischemic and five post-ischemic hearts. Five sets of differently radiolabeled microspheres were injected simultaneously in each heart (see methods). Each heart was divided into 72 segments, which were counted in a gamma counter for 5 min so that the number of counts detected from each microsphere was large enough so that variability due to statistical fluctuations in the number of disintegrations could be ignored. For each isotope i the gamma counter efficiency factor, ε_i, was measured using a reference standard whose activity level was specified by the isotope manufacturer. The expected number of disintegrations per microsphere, η_i, was calculated using data from the microsphere manufacturer. For each segment j the number of counts from each type of microsphere, c_i^j, was determined by decomposing the observed spectrum into a linear combination of spectra of reference isotope standards using a weighted least squares fit.

Combining this information, the number of microspheres labeled with isotope i trapped in segment j, n_i^j, was calculated:

$$n_i^j = \frac{c_i^j}{\varepsilon_i \eta_i}. \qquad \text{(A1)}$$

The fraction of microspheres trapped was calculated, also:

$$p_i^j = \frac{c_i^j}{C_i} = \frac{n_i^j}{N_i} \qquad \text{(A2)}$$

where $C_i = \sum_{j=1}^{J} c_i^j$ was the total number of counts from isotope i for the entire LV, $N_i = \sum_{j=1}^{J} n_i^j$ was the estimated total number of microspheres labeled with isotope i trapped in the LV, and J was the number of segments (i.e., $J = 72$).

Statistical Modeling. Assuming that the expected value of the entrapment fraction for segment j is the same for each isotope i and that the error in estimating the total number of trapped microspheres can be neglected, the expected value of the entrapment fraction, μ^j, is defined as follows:

$$\mu^j \triangleq E\left(p_i^j\right) = \frac{E\left(n_i^j\right)}{N_i}. \qquad \text{(A3)}$$

Using a Poisson model for microsphere entrapment, the variance of the entrapment fraction for isotope i in segment j is

$$Var\left(p_i^j\right) = \frac{Var\left(n_i^j\right)}{N_i^2} = \frac{E\left(n_i^j\right)}{N_i^2} = \frac{\mu^j}{N_i}. \qquad \text{(A4)}$$

Given models for the mean and variance of the entrapment fraction for each isotope i, an estimate of the expected entrapment fraction for segment j is obtained by defining a weighted least squares criterion in which squared differences between the observed and modeled entrapment fractions are inversely weighted by the modeled variances:

$$\left(X^j\right)^2 = \sum_{i=1}^{I} \frac{\left(p_i^j - \mu^j\right)^2 N_i}{\mu^j} = \sum_{i=1}^{I} \left(x_i^j\right)^2 \qquad \text{(A5)}$$

where $\left(x_i^j\right)^2 = \left(p_i^j - \mu^j\right)^2 N_i \Big/ \mu^j$ and I is the number of isotopes (i.e., $I = 5$). Minimizing this criterion with respect to the model parameter μ^j yields an estimate of the expected entrapment fraction, $\hat{\mu}^j$:

$$\hat{\mu}^j = \sqrt{\frac{\sum_{i=1}^{I} \left(p_i^j\right)^2 N_i}{\sum_{i=1}^{I} N_i}}. \qquad \text{(A6)}$$

Statistical Model Validation. Using simulated Poisson microsphere entrapment data it was verified that the criterion given by Equation A5 is distributed approximately as a chi-square random variable with $I-1$ degrees of freedom when $\hat{\mu}^j$ estimated by Equation A6 is substituted for μ^j in Equation A5 to obtain the following statistic:

$$\left(\hat{X}^j\right)^2 = \sum_{i=1}^{I} \frac{\left(p_i^j - \hat{\mu}^j\right)^2 N_i}{\hat{\mu}^j} = \sum_{i=1}^{I} \left(\hat{x}_i^j\right)^2. \qquad \text{(A7)}$$

For the case where a DD of 1 corresponds to 400 microspheres, 1.25 million independent Poisson random variables with mean values of 40 were generated to simulate the trapping of I=5 types of microspheres in J=250,000 heart sections having an expected DD of 0.1. For each heart section j the expected value of the entrapment fraction was estimated using Equation A6 and substituted into Equation A5 to yield Equation A7. The sample mean for each $\left(\hat{x}_i^j\right)^2$ term in the sum in Equation A7 was about 0.8, as expected given that their sum was distributed approximately as a chi-square random variable with $I-1$=4 degrees of freedom.

Similar calculations were then made using measured microsphere data obtained from 486 segments of the 7 hearts injected with 5 sets of microspheres. Sections were selected using the criterion that there should be evidence of flow such that the estimated activity for at least one of the isotopes was at least three times greater than its estimated uncertainty. Sections meeting this criterion had DD values ranging down to about 0.001 in post-ischemic hearts. Based on initial estimates of the total numbers of microspheres trapped in the LV (the N_i), the observed normalized deviations of the measurements (the $\hat{x}_i^j$ in *Eq. A7*) exceeded those predicted by the model by an average of about 27%. Possible explanations for the increased statistical fluctuation include errors in the average activity per microsphere, η_i, reported by the manufacturer; deviations in activity from sphere to sphere; errors in our measurements of the gamma counter efficiency factors, ε_i, due in part to errors in reference standard activities reported by the manufacturer; and sphere aggregation.

The estimates of the total numbers of microspheres trapped in the LV were then adjusted so that the average observed deviations were within 0.01% of those predicted by the model. Figure A1A contains a histogram (depicted as a bar graph) which shows the resulting distribution of normalized squared deviations (the $\left(\hat{x}_1^j\right)^2$ term in *Eq. A7*) for Sn-113-labeled microspheres. Figure A1A also contains a histogram (depicted using filled circles and error bars) which shows the shape of the distribution of normalized squared deviations obtained from the simulated Poisson entrapment data. There is good agreement between the measured and modeled distributions, following adjustment of the estimates of the total numbers of microspheres trapped in the LV. Figures A1B-A1E show the distributions of normalized squared deviations for Gd-153, Co-57, Ru-103, and Nb-95 labeled microspheres, which are also in good agreement with the model.

Interpreting these results as validation of a Poisson entrapment model, the following can be reiterated about the precision with which very low flows can be measured using few microspheres. Because the variance in the number of microspheres equals the expected number of microspheres, absolute precision increases as flow decreases and smaller absolute differences can be discriminated at low flow compared to high flow. For example, if a DD of 1 corresponds to 400 expected microspheres, then the standard deviation of 20 microspheres yields a standard deviation of 0.05 in the DD measurement (Figure 1). For a DD of 0.25, the expected number of microspheres is 100 and the standard deviation is only 10 microspheres. This reduces the standard deviation of the DD measurement by a factor of two so that the standard deviation is now only 0.025.

Confidence of Deposition Density Measurements. Formally, the variance of a DD measurement for isotope i in heart segment j (*Eq. 4*) is obtained from Equations 1, A2, and A4:

$$Var\left(d_i^j\right)=\left(\frac{M}{m^j N_i}\right)^2 Var\left(n_i^j\right)=\left(\frac{M}{m^j N_i}\right)^2 E\left(n_i^j\right)=\frac{M}{m^j N_i}E\left(d_i^j\right) \qquad \text{(A8)}$$

where it has been assumed that errors in measuring m^j can be neglected. Using this scaled Poisson model, the statistical significance of the difference between a DD measurement and a value of interest can be assessed. In particular, a number ranging between 0 and 1 can be assigned that quantifies the confidence that relative flow is above or below a certain level.

Approximating the scaled Poisson model with a Gaussian, the confidence that a DD measurement indicates a relative flow of at least α is given by the function

$$\rho_i^j(\alpha)=\Phi\left(\frac{d_i^j-\alpha}{\left(Md_i^j/m^j N_i\right)^{1/2}}\right) \qquad \text{(A9)}$$

where $\Phi(x)=\int_{-\infty}^{x}\frac{1}{\sqrt{2\pi}}\exp\left(-\frac{u^2}{2}\right)du$ is the cumulative distribution function for a Gaussian with zero mean and unit variance. Conversely, the confidence that relative flow is less than α is 1- $\rho_i^j(\alpha)$. Based on this single measurement, a Bernoulli random variable, b_i^j, can be used to model the outcomes of repeatedly measuring DD in a heart segment for which the expected value is d_i^j. The random variable b_i^j either takes a value of 1 with probability 1- $\rho_i^j(\alpha)$ to indicate that DD is less than α, or takes a value of 0 with probability $\rho_i^j(\alpha)$ to indicate that DD is at least α. Thus, the expected total number of segments for which DD is less than α is

$$E\left(\sum_{j=1}^{J} b_i^j\right) = \sum_{j=1}^{J}\left[1-\rho_i^j(\alpha)\right] \qquad \text{(A10)}$$

where it has been assumed that the DD measurements are independent of one another. The associated variance is

$$Var\left(\sum_{j=1}^{J} b_i^j\right) = \sum_{j=1}^{J}\rho_i^j(\alpha)\left[1-\rho_i^j(\alpha)\right] \qquad \text{(A11)}$$

When analyzing post-ischemic segments for impaired reflow, the threshold, α, was set to 0.1 and Equation A10 was used to estimate the number of segments having impaired reflow. An estimate of uncertainty in the number of segments having impaired reflow was obtained as the square root of the variance given by Equation A11.

Summary. The Poisson statistical model for microsphere entrapment was validated and used to determine the confidence with which radiolabeled microsphere deposition density measurements indicated impaired reflow. As predicted by the model, absolute precision increases as flow decreases. Smaller absolute differences can be discriminated at low flow, compared to high flow.

To apply the Poisson model, an accurate estimate of the total number of microspheres trapped in the heart is needed. When using radiolabeled microspheres it is beneficial to perform experiments in which differently radiolabeled sets of microspheres are injected simultaneously, so that calibration factors can be checked and adjusted, if need be, for use in subsequent experiments in which only one set is injected at a time.

ACKNOWLEDGMENTS

This work was supported by National Heart, Lung and Blood Institute grants P01 HL25840 and R01 HL60877, and by the Director, Office of Science, Office of Biological and Environmental Research, Medical Sciences Division of the U.S. Department of Energy under Contract No. DE-AC03-76SF00098.

REFERENCES

1. **Anderson PG, Bishop SP, and Digerness SB**. Transmural progression of morphologic changes during ischemic contracture and reperfusion in the normal and hypertrophied rat heart. *Am J Pathol* 129: 152-67, 1987.

2. **Apstein CS, Mueller M, and Hood WB, Jr.** Ventricular contracture and compliance changes with global ischemia and reperfusion, and their effect on coronary resistance in the rat. *Circ Res* 41: 206-17, 1977.

3. **Austin RE, Jr., Aldea GS, Coggins DL, Flynn AE, and Hoffman JIE**. Profound spatial heterogeneity of coronary reserve. Discordance between patterns of resting and maximal myocardial blood flow. *Circ Res* 67: 319-31, 1990.

4. **Austin RE, Jr., Hauck WW, Aldea GS, Flynn AE, Coggins DL, and Hoffman JIE**. Quantitating error in blood flow measurements with radioactive microspheres. *Am J Physiol* 257: H280-8, 1989.

5. **Austin RE, Jr., Smedira NG, Squiers TM, and Hoffman JIE**. Influence of cardiac contraction and coronary vasomotor tone on regional myocardial blood flow. *Am J Physiol* 266: H2542-53, 1994.

6. **Bassingthwaighte JB, Beard DA, and Li Z**. The mechanical and metabolic basis of myocardial blood flow heterogeneity. *Basic Res Cardiol* 96: 582-94., 2001.

7. **Bassingthwaighte JB, Malone MA, Moffett TC, King RB, Chan IS, Link JM, and Krohn KA**. Molecular and particulate depositions for regional myocardial flows in sheep. *Circ Res* 66: 1328-44, 1990.

8. **Bassingthwaighte JB, Malone MA, Moffett TC, King RB, Little SE, Link JM, and Krohn KA**. Validity of microsphere depositions for regional myocardial flows. *Am J Physiol* 253: H184-93, 1987.

9. **Bassingthwaighte JB, Raymond GM, and Chan JI**. Principles of tracer kinetics. In: *Nuclear Cardiology: State of the Art and Future Directions*, edited by Zaret BL and Beller GA. St. Louis: Mosby-Year Book, Inc., 1993, p. 3-23.

10. **Bogaert J and Rademakers FE**. Regional nonuniformity of normal adult human left ventricle. *Am J Physiol Heart Circ Physiol* 280: H610-20, 2001.

11. **Buckberg GD, Luck JC, Payne DB, Hoffman JIE, Archie JP, and Fixler DE**. Some sources of error in measuring regional blood flow with radioactive microspheres. *Journal of Applied Physiology* 31: 598-604, 1971.

12. **Bussemaker J, Groeneveld AB, Teerlink T, Hennekes M, Westerhof N, and van Beek JH**. Low- and high-blood flow regions in the normal pig heart are equally vulnerable to ischaemia during partial coronary stenosis. *Pflugers Arch* 434: 785-94, 1997.

13. **Clarke K, Stewart LC, Neubauer S, Balschi JA, Smith TW, Ingwall JS, Nédélec JF, Humphrey SM, Kléber AG, and Springer CS, Jr.** Extracellular volume and transsarcolemmal proton movement during ischemia and reperfusion: a 31P NMR spectroscopic study of the isovolumic rat heart. *NMR in Biomedicine* 6: 278-86, 1993.

14. **Flynn AE, Coggins DL, Austin RE, Muehrcke DD, Aldea GS, Goto M, Doucette JW, and Hoffman JI**. Nonuniform blood flow in the canine left ventricle. *J Surg Res* 49: 379-84, 1990.

15. **Fung YC**. Stochastic flow in capillary blood vessels. *Microvasc Res* 5: 34-48., 1973.

16. **Gavin JB, Maxwell L, and Sage MD**. Interrelationships of Ultrastructure and Function in the Microvasculature of Normal and Ischaemic Myocardium. *J Electron Microsc Tech* V19: 429-438, 1991.

17. **Ghaleh B, Shen Y-T, and Vatner SF**. Spatial heterogeneity of myocardial blood flow presages salvage versus necrosis with coronary artery reperfusion in conscious baboons. *Circulation* 94: 2210-2215, 1996.

18. **Gorman MW and Sparks HV, Jr.** Progressive coronary vasoconstriction during relative ischemia in canine myocardium. *Circ Res* 51: 411-20., 1982.

19. **Gorman MW, Wangler RD, and Sparks HV**. Distribution of perfusate flow during vasodilation in isolated guinea pig heart. *Am J Physiol* 256: H297-301, 1989.

20. **Hearse DJ, Maxwell L, Saldanha C, and Gavin JB**. The Myocardial Vasculature During Ischemia and Reperfusion - a Target for Injury and Protection. *J Mol Cell Cardiol* V25: 759-800, 1993.

21. **Heineman FW and Grayson J**. Transmural distribution of intramyocardial pressure measured by micropipette technique. *Am J Physiol* 249: H1216-23, 1985.

22. **Humphrey SM and Gavin JB**. The effect of coronary pressure on contracture and vascular perfusion in the hypoxic isolated rat heart. *Bas Res Cardiol* 79: 350-62, 1984.

23. **Humphrey SM, Gavin JB, and Herdson PB**. The relationship of ischemic contracture of vascular reperfusion in the isolated rat heart. *J Mol Cell Cardiol* 12: 1397-406, 1980.

24. **Humphrey SM, Thomson RW, and Gavin JB**. The effect of an isovolumic left ventricle on the coronary vascular competence during reflow after global ischemia in the rat heart. *Circ Res* 49: 784-91, 1981.

25. **Humphrey SM, Thomson RW, and Gavin JB**. The influence of the no-reflow phenomenon on reperfusion and reoxygenation damage and enzyme release from anoxic and ischaemic isolated rat hearts. *J Mol Cell Cardiol* 16: 915-29, 1984.

26. **Jennings RB, Reimer KA, and Steenbergen C**. Myocardial ischemia revisited. The osmolar load, membrane damage, and reperfusion. *J Mol Cell Cardiol* 18: 769-80, 1986.

27. **King RB, Bassingthwaighte JB, Hales JR, and Rowell LB**. Stability of heterogeneity of myocardial blood flow in normal awake baboons. *Circ Res* 57: 285-95, 1985.

28. **Kloner RA, Ganote CE, and Jennings RB**. The "no-reflow" phenomenon after temporary coronary occlusion in the dog. *J Clin Invest* 54: 1496-508, 1974.

29. **Kolocassides KG, Galinanes M, and Hearse DJ**. Dichotomy of ischemic preconditioning: improved postischemic contractile function despite intensification of ischemic contracture. *Circulation* 93: 1725-33, 1996.

30. **Marcus ML, Kerber RE, Ehrhardt J, and Abboud FM**. Three dimensional geometry of acutely ischemic myocardium. *Circulation* 52: 254-63, 1975.

31. **Marshall RC**. Correlation of contractile dysfunction with oxidative energy production and tissue high energy phosphate stores during partial coronary flow disruption in rabbit heart. *J Clin Invest* 82: 86-95, 1988.

32. **Marshall RC, Powers-Risius P, Reutter BW, Taylor SE, VanBrocklin HF, Huesman RH, and Budinger TF**. Kinetic analysis of 125I-iodorotenone as a deposited myocardial flow tracer: comparison with 99mTc-sestamibi. [Comment In: J Nucl Med. 2001 Feb;42(2):282-4 UI: 21084274]. *J Nucl Med* 42: 272-81, 2001.

33. **Marshall RC, Taylor SE, Powers-Risius P, Reutter BW, Kuruc A, Coxson PG, Huesman RH, and Budinger TF**. Kinetic analysis of rubidium and thallium as deposited myocardial blood flow tracers in isolated rabbit heart. *Am J Physiol* 272: H1480-90, 1997.

34. **Maxwell L and Gavin J**. Anti-oxidant therapy improves microvascular ultrastructure and perfusion in postischemic myocardium. *Microvasc Res* 43: 255-66., 1992.

35. **Maxwell L and Gavin JB**. The role of post-ischaemic reperfusion in the development of microvascular incompetence and ultrastructural damage in the myocardium. *Bas Res Cardiol* 86: 544-553, 1991.

36. **Mehta JL, Lawson DL, and Nichols WW**. Attenuated coronary relaxation after reperfusion: Effects of superoxide dismutase and TxA2 inhibitor U 63557A. *Am J Physiol* 257: H1240-H1246, 1989.

37. **Merrill G, McConnell P, Vandyke K, and Powell S**. Coronary and myocardial effects of acetaminophen: Protection during ischemia-reperfusion. *Am J Physiol* 280: H2631-H2638, 2001.

38. **Nichols WW, Mehta JL, Donnelly WH, Lawson D, Thompson L, and Ter Riet M**. Reduction in coronary vasodilator reserve following coronary occlusion and reperfusion in anesthetized dog: Role of

endothelium-derived relaxing factor, myocardial neutrophil infiltration and prostaglandins. *J Mol Cell Cardiol* 20: 943-954, 1988.

39. **Nose Y, Nakamura T, and Nakamura M**. The microsphere method facilitates statistical assessment of regional blood flow. *Bas Res Cardiol* 80: 417-29, 1985.

40. **Pelc LR, Garancis JC, Gross GJ, and Warltier DC**. Alteration of endothelium-dependent distribution of myocardial blood flow after coronary occlusion and reperfusion. *Circulation* 81: 1928-37., 1990.

41. **Pelc LR, Gross GJ, Kampine JP, and Warltier DC**. Mechanisms of enhanced canine subendocardial perfusion. A comparison of adenosine triphosphate and sodium nitroprusside. *Anesth Analg* 67: 514-20., 1988.

42. **Polissar NL, Stanford DC, and Glenny RW**. The 400 microsphere per piece "rule" does not apply to all blood flow studies. *Am J Physiol Heart Circ Physiol* 278: H16-25, 2000.

43. **Rabbany SY, Kresh JY, and Noordergraaf A**. Intramyocardial pressure: interaction of myocardial fluid pressure and fiber stress. *Am J Physiol* 257: H357-64, 1989.

44. **Schwanke U, Deussen A, Heusch G, and Schipke JD**. Heterogeneity of local myocardial flow and oxidative metabolism. *Am J Physiol* 279: H1029-H1035, 2000.

45. **Steenbergen C, Murphy E, Watts JA, and London RE**. Correlation between cytosolic free calcium, contracture, ATP, and irreversible ischemic injury in perfused rat heart. *Circ Res* 66: 135-46, 1990.

46. **Takeo S, Liu JX, Tanonaka K, Nasa Y, Yabe K, Tanahashi H, and Sudo H**. Reperfusion at reduced flow rates enhances postischemic contractile recovery of perfused heart. *Am J Physiol* 268: H2384-95, 1995.

47. **Tilton RG, Larson KB, Udell JR, Sobel BE, and Williamson JR**. External detection of early microvascular dysfunction after no-flow ischemia followed by reperfusion in isolated rabbit hearts. *Circ Res* 52: 210-25., 1983.

48. **Tsao PS and Lefer AM**. Time course and mechanism of endothelial dysfunction in isolated ischemic-and hypoxic-perfused rat hearts. *Am J Physiol* 259: H1660-H1666, 1990.

49. **Vanbenthuysen KM, McMurtry IF, and Horwitz LD**. Reperfusion after acute coronary occlusion in dogs impairs endothelium-dependent relaxation to acetylcholine and augments contractile reactivity in vitro. *J Clin Invest* 79: 265-274, 1987.

50. **Versluis JP, Heslinga JW, Sipkema P, and Westerhof N**. Microvascular pressure measurement reveals a coronary vascular waterfall in arterioles larger than 110 microm. *Am J Physiol Heart Circ Physiol* 281: H1913-8., 2001.

51. **Wolpers HG, Hoeft A, Korb H, Lichtlen PR, and Hellige G**. Heterogeneity of myocardial blood flow under normal conditions and its dependence on arterial PO2. *Am J Physiol* 258: H549-55, 1990.

52. **Woodman OL**. Approaches to the prevention of coronary vascular dysfunction caused by myocardial ischaemia and reperfusion. *Curr Pharm Des* 5: 1077-1087, 1999.

FIGURE LEGENDS

Fig. 1. Depiction of increase in absolute precision with decreasing flow. Poisson probability distributions are shown for measurements involving 400, 100, and 25 expected microspheres, corresponding to deposition densities of 1 ± 0.05, 0.25 ± 0.025, and 0.0625 ± 0.0125, respectively. Decreasing flow by a factor of four reduces the standard deviation by a factor of two.

Fig. 2. Binned values of deposition density expressed as percent of whole LV mass (*A*); subendocardium mass (*B*); and subepicardium mass (*C*). The data are from the pre-ischemia MS distributions of the 60 min ischemia plus 50 min reperfusion experiments (n = 5), the first MS distribution of the control experiments (n = 5), and the non-ischemia 5 MS experiments (n = 2). For the 5 MS experiments, only Sn-113 labeled microspheres were included. Of the 864 segments included in this illustration, six had deposition densities less than 0.1.

Fig. 3. The sum of the section weights in 0.1 increments of deposition density expressed as the percent of the total LV, subendocardium, or subepicardium mass. *A*: early post-ischemia, whole LV. *B*: late post-ischemia, whole LV. *C*: early post-ischemia, subendocardium. *D*: late post-ischemia, subendocardium. *E*: early post-ischemia, subepicardium. *F*: late post-ischemia, subepicardium. In C-F, the DDs have been renormalized so that the mean DD in the subendocardium and subepicardium considered individually are each 1.

Fig. 4. Relative dispersion vs. the number of subendocardial (open triangles and dashed line), subepicardial (squares and dotted line), and whole LV (solid circles and solid line) segments with impaired flow following 60 min ischemia (5 experiments). *A:* Early reperfusion. *B*: Late reperfusion. The equations for the linear regression lines are shown in the panels.

Fig. 5. The relationship between end-ischemic rest pressure and relative dispersion (*A*) and the number of segments with impaired flow (*B*). Data are from Protocols 1 and 3 hearts (see Table 1). The relative dispersion values and sections with impaired reflow in Protocol 1 hearts were computed using a single isotope (Sn-113). The equations for the linear regressions are shown in each panel.

Fig. A1. Measured and modeled distributions for normalized squared deviations of entrapment fractions for microspheres labeled with (A) Sn-113; (B) Gd-153; (C) Co-57; (D) Ru-103; and (E) Nb-95. Bar graphs depict the measured distributions and filled circles depict the modeled distribution obtained from simulated Poisson entrapment data. Error bars depict a range corresponding to plus or minus one standard deviation, where the standard deviation has been calculated as the square root of the number of simulated segments in the model histogram bin. The horizontal axis has been truncated at a value beyond which lies only about 1% of the simulated segments.

Table 1. *LV function and perfusion values at the time of microsphere introduction*

Group	Flow, $ml \cdot min^{-1} \cdot g^{-1}$	DP, mmHG	RP, mmHG	PP, mmHG	CVR, $mmHg/ml \cdot min^{-1} \cdot g^{-1}$
			Non-ischemia		
5 MS Controls (n = 2; Protocol 1)					
15 min post equilibration	1.4 ± 0.1	80 ± 3	6 ± 1	56 ± 4	41 ± 6
Non-ischemic Control (n = 5; Protocol 2)					
15 min post equilibration	1.4 ± 0.4	79 ± 4	6 ± 4	61 ± 9	49 ± 27
1 hr post equilibration	1.4 ± 0.3	80 ± 9	5 ± 4	63 ± 12	52 ± 28
2 hr post equilibration	1.4 ± 0.3	79 ± 4	6 ± 4	71 ± 14[a]	58 ± 31
60 min Ischemia (n = 5; Protocol 3)					
Pre-ischemia	1.3 ± 0.2	87 ± 13	5 ± 2	61 ± 8	48 ± 14
			Post-ischemia		
60 min Ischemia (n = 5; Protocol 3)					
Early reperfusion	1.2 ± 0.3	28 ± 11[b]	48 ± 33[c]	79 ± 19[d]	69 ± 23
Late reperfusion	1.1 ± 0.2[e]	44 ± 15[f]	46 ± 28[c]	80 ± 16[d]	78 ± 24
5 MS Post-ischemia (n = 4[g]; Protocol 1)					
Early reperfusion	1.1 ± 0.2	21 ± 12	53 ± 20	77 ± 11	75 ± 24

Values are means ± SDs; DP, developed pressure; RP, rest pressure; PP, perfusion pressure; CVR, coronary vascular resistance; n, number of hearts. [a]$P < 0.03$ vs. 15 min; [b]$P < 0.001$ vs. pre-ischemia; [c]P

< 0.05 vs. pre-ischemia; [d]*P* < 0.05 vs. pre-ischemia; [e]*P* < 0.03 vs. early reperfusion, [f]P < 0.02 vs. early reperfusion. [g]In one heart, systolic performance was depressed during equilibration (DP < than 60 mmHg), therefore, ventricular performance and perfusion data were excluded, although the data on microsphere reproducibility were considered valid and were analyzed.

Table 2. *Relative dispersion and blood flow distribution for non-ischemic control hearts*

Injection Time	Relative Dispersion			Relative Blood Flow	
post equilibration	Whole LV	Subendocardium	Subpicardium	Endo:Epi	Endo–Epi,
15 min	0.39 ± 0.07	0.33 ± 0.04	0.43 ± 0.13	1.39 ± 0.19	0.22 ± 0.09
60 min	0.38 ± 0.07	0.32 ± 0.07	0.39 ± 0.10	1.41 ± 0.23	0.26 ± 0.11
120 min	0.37 ± 0.05	0.30 ± 0.05	0.34 ± 0.04	1.53 ± 0.19*	0.36 ± 0.11*

Values are means ± SDs for five experiments; Endo:Epi, ratio of subendocardium to subepicardium deposition density; Endo-Epi, subendocardium minus subepicardium deposition density. *$P < 0.03$ vs. 15 min.

Table 3. *Relative dispersion and relative blood flow for 60-min ischemia hearts*

Injection time	Relative Dispersion			Relative Blood Flow
	Whole LV	Subendocardium	Subepicardium	Endo–Epi,
Pre-ischemia	0.37 ± 0.07	0.30 ± 0.09	0.38 ± 0.08	0.19 ± 0.24
Early reperfusion	0.92 ± 0.41*	1.28 ± 0.74*	0.69 ± 0.22*	-0.62 ± 0.57*
Late reperfusion	0.70 ± 0.22*	1.06 ± 0.55*	0.43 ± 0.57	-0.53 ± 0.56

Values are means ± SDs for five experiments; microspheres were injected at three different points during the experiment: pre-ischemia, early (20 min), and late (50 min) during reperfusion. Endo–Epi, subendocardium minus subepicardium deposition density. Only the difference in subendocardial and subepicardial deposition density are shown because a few subepicardial segments had severely impaired reflow. $^{*}P < 0.05$ vs. pre-ischemia.

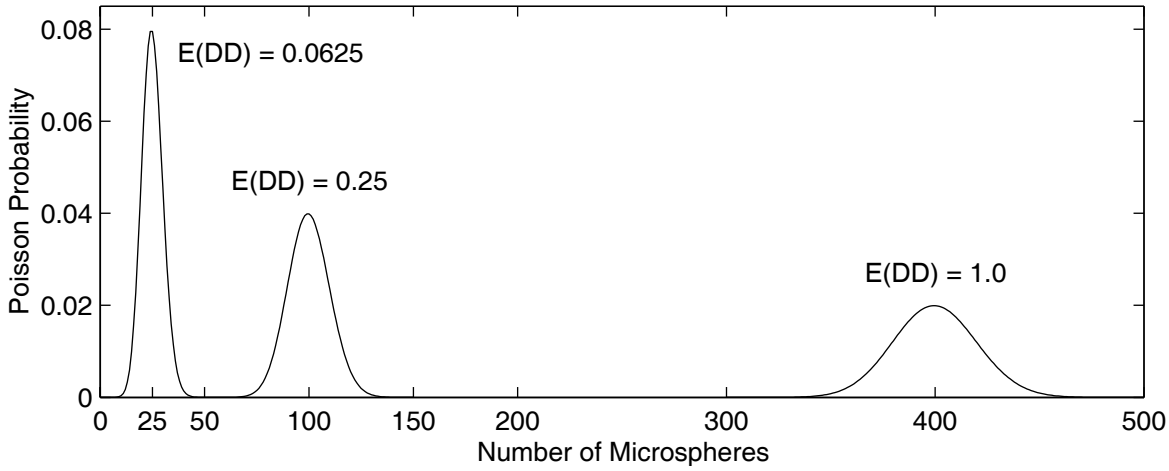
0.08
0.06
0.04
0.02
0
Poisson Probability
E(DD) = 0.0625
E(DD) = 0.25
E(DD) = 1.0
0
25
50
100
150
200
300
400
500
Number of Microspheres

Fig. 1

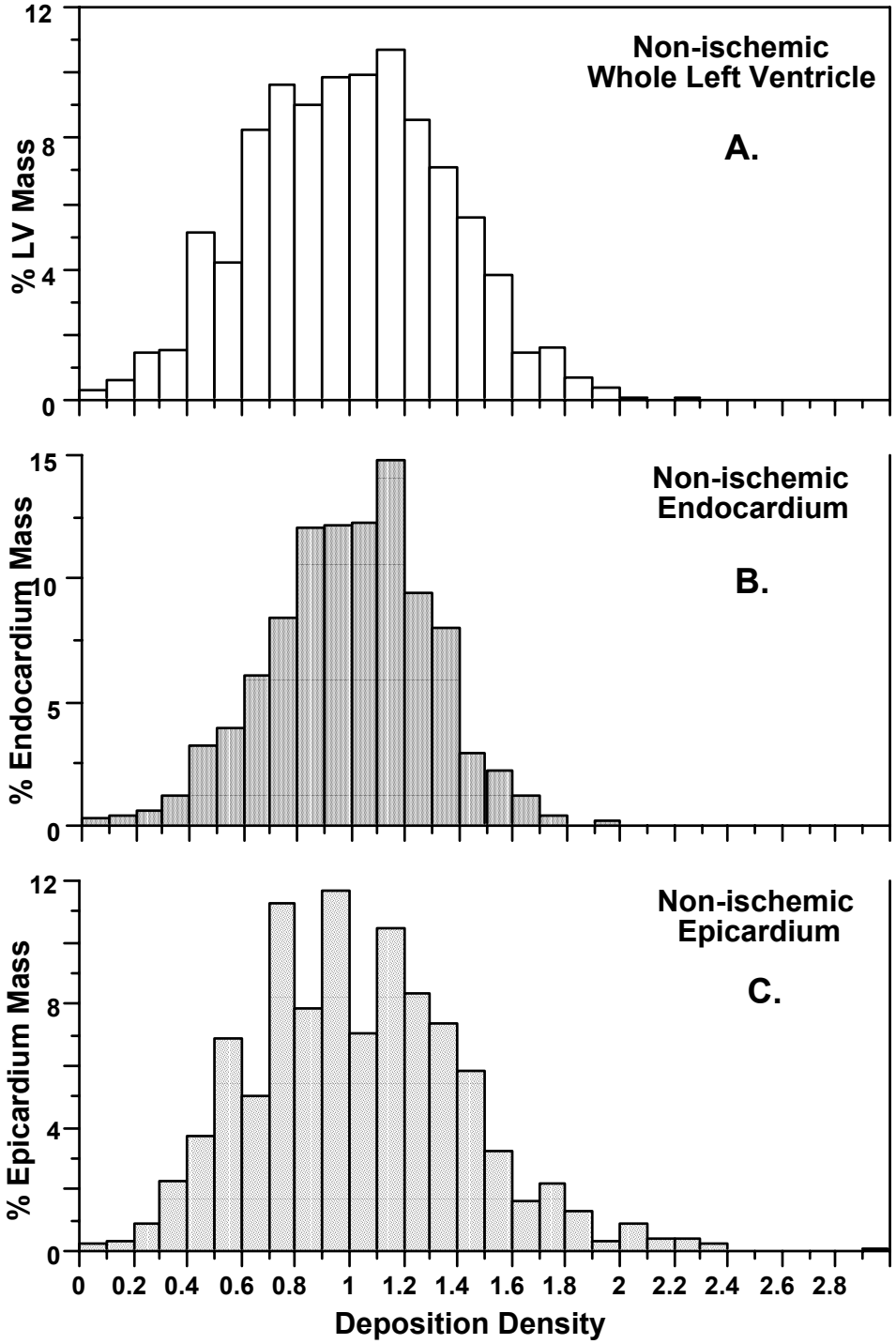
Non-ischemic
Whole Left Ventricle
A.
% LV Mass
12
8
4
0
Non-ischemic
Endocardium
B.
% Endocardium Mass
15
10
5
0
Non-ischemic
Epicardium
C.
% Epicardium Mass
12
8
4
0
0 0.2 0.4 0.6 0.8 1 1.2 1.4 1.6 1.8 2 2.2 2.4 2.6 2.8
Deposition Density

Fig. 2

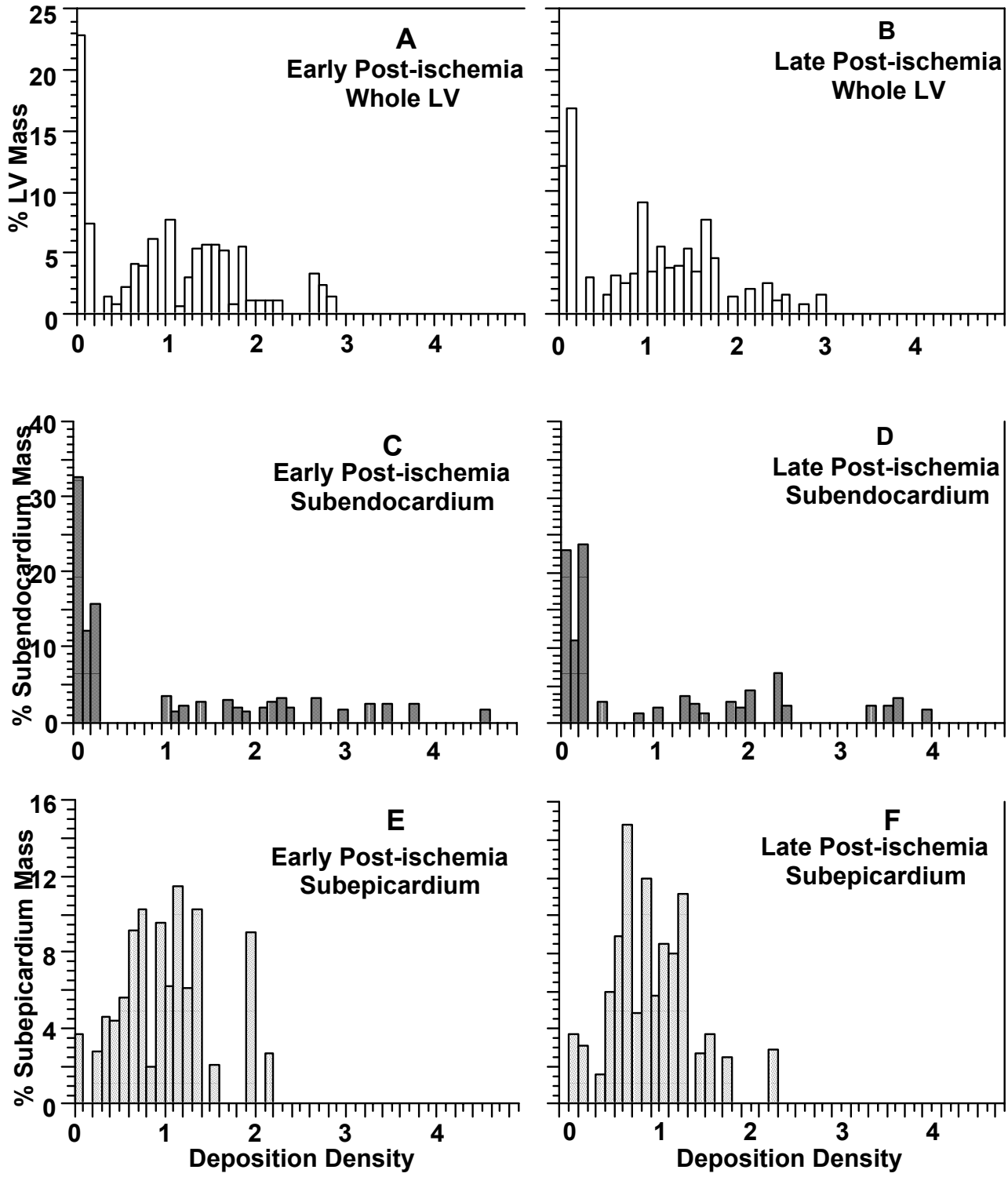
A
Early Post-ischemia
Whole LV
B
Late Post-ischemia
Whole LV
% LV Mass
C
Early Post-ischemia
Subendocardium
D
Late Post-ischemia
Subendocardium
% Subendocardium Mass
E
Early Post-ischemia
Subepicardium
F
Late Post-ischemia
Subepicardium
% Subepicardium Mass
Deposition Density
Deposition Density

Fig. 3

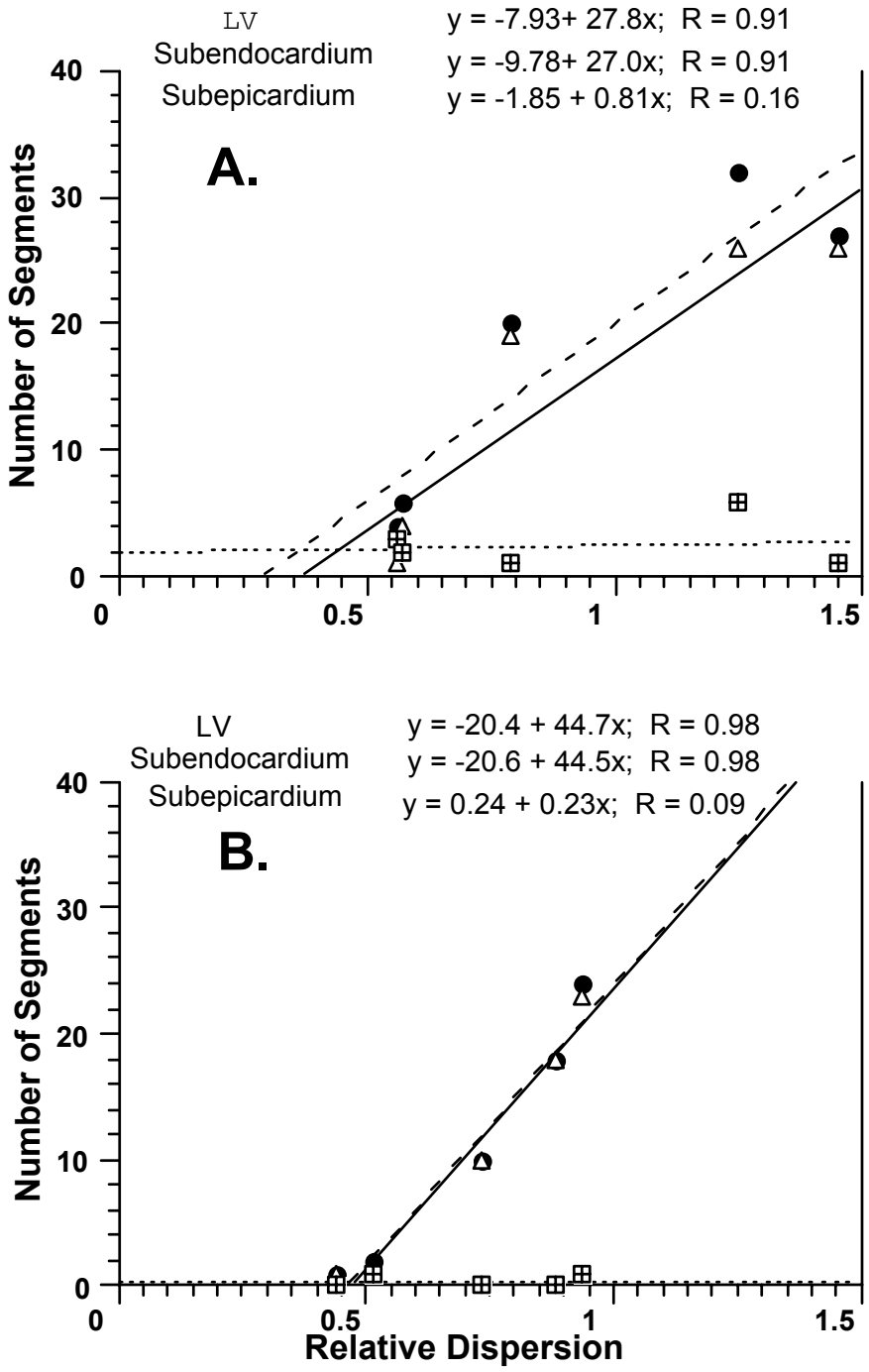
LV
Subendocardium
Subepicardium
y = -7.93+ 27.8x; R = 0.91
y = -9.78+ 27.0x; R = 0.91
y = -1.85 + 0.81x; R = 0.16
A.
Number of Segments
40
30
20
10
0
0
0.5
1
1.5
LV
Subendocardium
Subepicardium
y = -20.4 + 44.7x; R = 0.98
y = -20.6 + 44.5x; R = 0.98
y = 0.24 + 0.23x; R = 0.09
B.
Number of Segments
Relative Dispersion

Fig.4

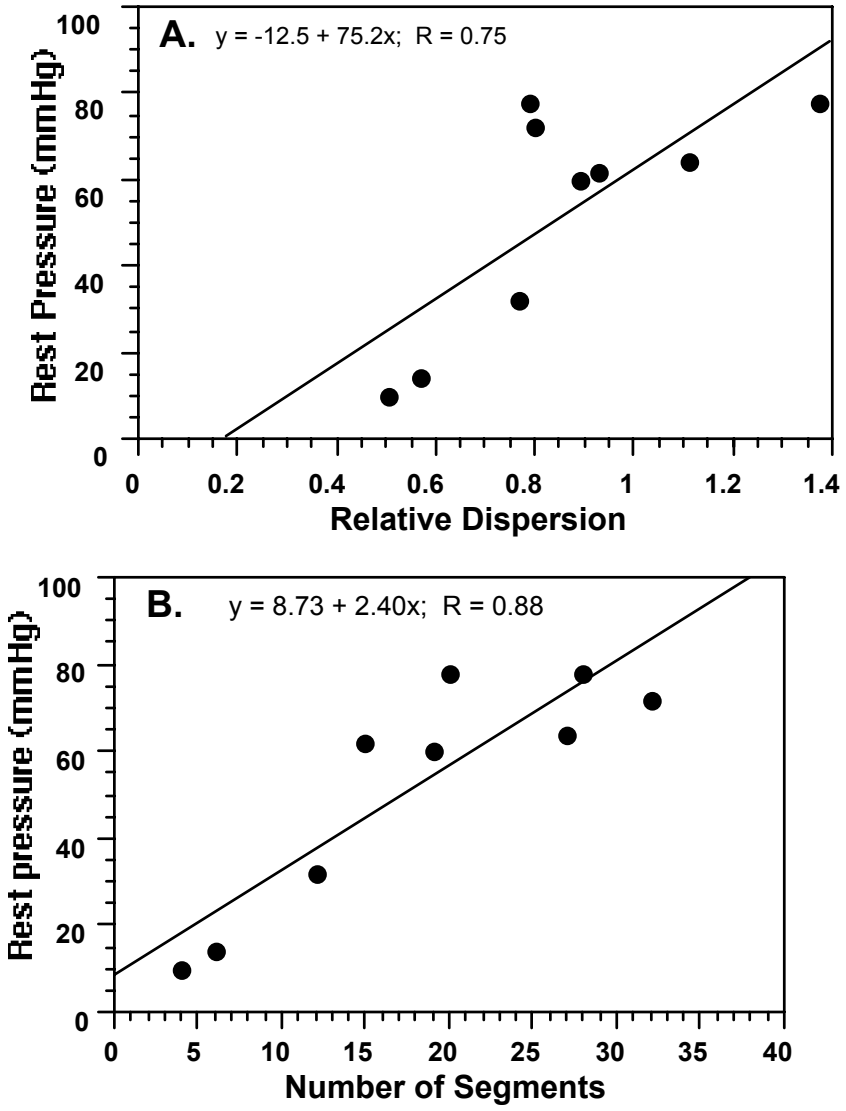
A.
y = -12.5 + 75.2x; R = 0.75
Rest Pressure (mmHg)
Relative Dispersion
0
20
40
60
80
100
0
0.2
0.4
0.6
0.8
1
1.2
1.4
B.
y = 8.73 + 2.40x; R = 0.88
Rest pressure (mmHg)
Number of Segments
0
20
40
60
80
100
0
5
10
15
20
25
30
35
40

Fig. 5

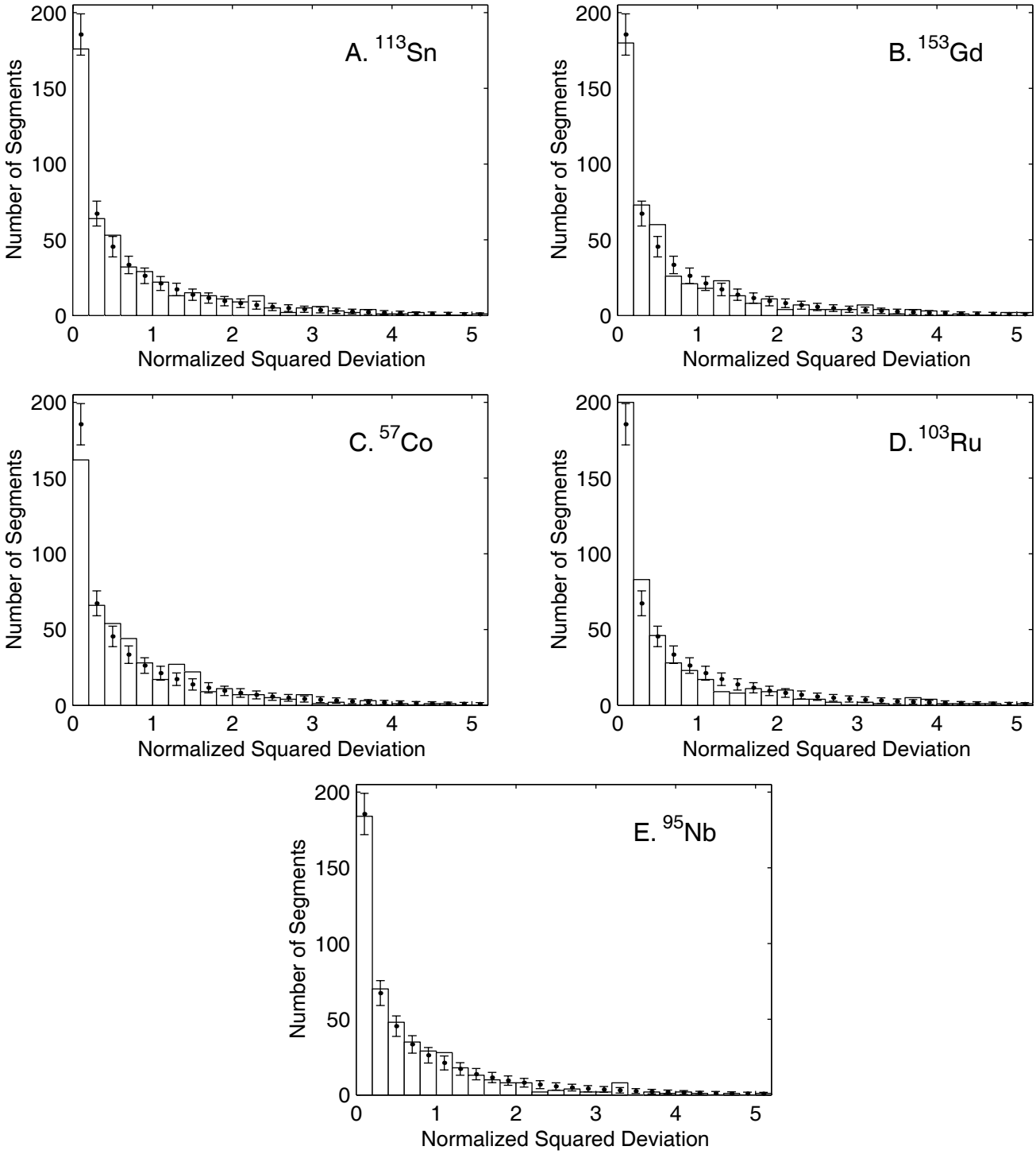
A. ^{113}Sn
B. ^{153}Gd
C. ^{57}Co
D. ^{103}Ru
E. ^{95}Nb
Number of Segments
Normalized Squared Deviation
0
50
100
150
200
0
1
2
3
4
5

Fig. A1